ELEMENTS OF PHYSICS WITH A PHOTON COLLIDER*

M.M. Mühlleitner

Laboratoire d'Annecy-Le-Vieux de Physique Théorique, LAPTH
Annecy-Le-Vieux, France

P.M. Zerwas

Deutsches Elektronen-Synchrotron, DESY, Hamburg, Germany

(Received February 16, 2006)

After a brief description of the basic principle of a photon collider, we summarize the physics potential of such a facility at high energies. Unique opportunities are provided in supersymmetric theories for the discovery of heavy scalar and pseudoscalar Higgs bosons as well as selectrons and e-sneutrinos.

PACS numbers: 12.15.–y, 12.38.–t, 12.60.–i

1. Introduction

Linear colliders, LC, can be operated in several modes among which the $e\gamma$ and $\gamma\gamma$ modes provide a wide field of physics opportunities, including unique experimental solutions to fundamental problems [1, 2]. By means of Compton back-scattering of laser light, almost the entire energy of electrons/positrons at a linear collider can be transferred to photons [3] so that $e\gamma$ and $\gamma\gamma$ processes can be studied for energies close to the TeV scale. The luminosities are expected to be about one third of the e^+e^- luminosity in the high energy regime [1,2]. Since the cross sections for $e\gamma$ and $\gamma\gamma$ processes are in general significantly larger than the cross sections for e^+e^- annihilation processes, the event rates will be of similar size in the three LC modes. Various options of choosing the photon polarizations, circular and linear, allow unique experimental analyses of particle properties and interactions.

* Presented by P.M. Zerwas at the PLC2005 Workshop, 5–8 September 2005, Kazimierz, Poland.

A rich spectrum of interesting physics problems can be studied experimentally at a photon collider operating at energies up to a TeV:

Higgs physics: The formation of Higgs bosons in $\gamma\gamma$ collisions can be used to measure precisely the Higgs–$\gamma\gamma$ coupling [4,5]. Since photons do not couple directly to neutral Higgs bosons, the coupling is mediated by virtual charged particle loops, being sensitive to scales potentially far beyond the Higgs mass. In the supersymmetry sector, $\gamma\gamma$ formation allows us to generate heavy scalar and pseudoscalar Higgs bosons [6,7] in a wedge centered around medium $\tan\beta$ values, in which no other collider, neither the LHC nor the LC e^+e^- mode, gives access to the spectrum of heavy Higgs bosons. Near degeneracy of the scalar and pseudoscalar Higgs bosons will give rise to large asymmetry effects in γ polarization experiments [8,9] if CP is broken in the Higgs sector.

Supersymmetry: A photon collider provides unique opportunities also in the genuine supersymmetric particle sector. In $e\gamma$ collisions the production of selectrons in association with light neutralinos can give access to selectron masses in excess to pair production in the LC $e^\pm e^-$ modes [10]. Similarly the production of e-sneutrinos in association with charginos may be used to study the properties of sneutrinos [11].

Static electromagnetic parameters: The large production cross sections for charged particles in $\gamma\gamma$ collisions can be exploited to determine their static electromagnetic parameters with high precision. The measurement of the electromagnetic multi-pole moments can be performed in a pure electromagnetic environment without interference with weak effects. Examples are the magnetic dipole moment of the top quark [12], and the magnetic dipole moment and electric quadrupole moment of the charged $W^\pm$ bosons [13,14].

QCD: Among the QCD problems which can be addressed at a high energy photon collider, two problems are of particular interest. The total $\gamma\gamma$ fusion cross section to hadrons is built up by a mixture of non-perturbative and perturbative interactions including the difficult transition zone between the two regimes. Of tantamount importance is the analysis of the quark and gluon content of the photon [15–17]. These parton distributions had been predicted to be very different from nucleons, with characteristic properties governed by asymptotic freedom.

Varia: Experiments at a photon collider open many other windows for interesting search experiments, extending from heavy Majorana neutrinos, see *e.g.* Ref. [18], to excited electrons. The key is the character of the photon as an almost pure energy quantum which is very effective in exciting new degrees of freedom. As a result, new particles can be generated with masses very close to the total energy in the system, most transparent for the electron excitation tower $\{e^*\}$ of compositeness models in $e\gamma$ collisions.

Some of these elements will be reviewed in the third to fifth section of this report after the basic principle of photon colliders is briefly described in the next section.

2. The basic principle

In e^+e^-/e^-e^- linear colliders nearly the entire electron/positron energy can be transferred to photons by Compton back-scattering of laser light. This method has been proposed in Refs. [3]. The scheme is based on two elements. Kinematically, by energy-momentum conservation, a low-energy laser photon must carry away almost the entire energy when scattered backward in a collision with a high-energy electron/positron. Dynamically, the cross section is maximal, due to the u-channel exchange of electrons/positrons

$$A_u \sim \frac{1}{(u - m_e^2)} \sim \frac{1}{(1 + \beta_e \cos\theta)}\,, \tag{1}$$

for back-scattering of the photons.

2.1. Photon energy

The spectrum is described in detail by the shape function

$$F(y) = \frac{1}{1-y} + (1-y) - 4r(1-r) + 2\lambda_e P_c x r(1-2r)(2-y)\,, \tag{2}$$

where

$$y = \frac{E_\gamma}{E_e} \tag{3}$$

denotes the fraction of energy transferred from the electron/positron to the photon and r abbreviates the ratio $r = y/(1-y)x$. The helicities λ_e and P_c refer to the incoming electrons/positrons and laser photons, respectively. The parameter

$$x = \frac{4E_e\omega_\gamma}{m_e^2}\,, \tag{4}$$

measures the invariant energy (squared) in units of the electron mass, with ω_γ denoting the laser γ energy. x determines the upper limit of the final photon energy

$$E_\gamma^{\max} = \frac{1}{1 + x^{-1}}\, E_e\,. \tag{5}$$

The larger the value for x is chosen the more energy can be transferred to the photon. However, to suppress electron–positron pair production in collisions of the high-energy photons, already generated in the Compton process, with the numerous left-over laser photons, an upper bound on $x \leq 2/(\sqrt{2}-1) \simeq 4.8$ must be imposed.

For typical values $E_e = 250\,\text{GeV}$ and $\omega_\gamma = 1.17\,\text{eV}$ more than 80% of the electron/positron energy can be transferred to the photon,

$$E_\gamma^{\max} = 0.82\, E_e\,, \tag{6}$$

generating a photon–photon invariant energy of more than 800 GeV at a 1 TeV $e^\pm e^-$ collider.

By choosing opposite helicities for the initial electron/positron beams and the laser photons, *i.e.* $2\lambda_e P_c = -1$, the spectrum of the final-state photons can be sharpened dramatically, *cf.* Fig. 1 (left). The γ conversion of electron beams for which a polarization degree of 95% may eventually be achieved, is therefore preferable over positron beams where an upper limit of about 60% is expected.

Non-linear effects reduce the upper energy slightly, but give rise to a large number of photons at the lower end of the spectrum. Higher harmonics, on the other hand, lead to a shallow increase of the upper energy limit, *cf.* Fig. 1 (right). The main characteristics of the high-energy photon spectrum, however, remain largely unaltered.

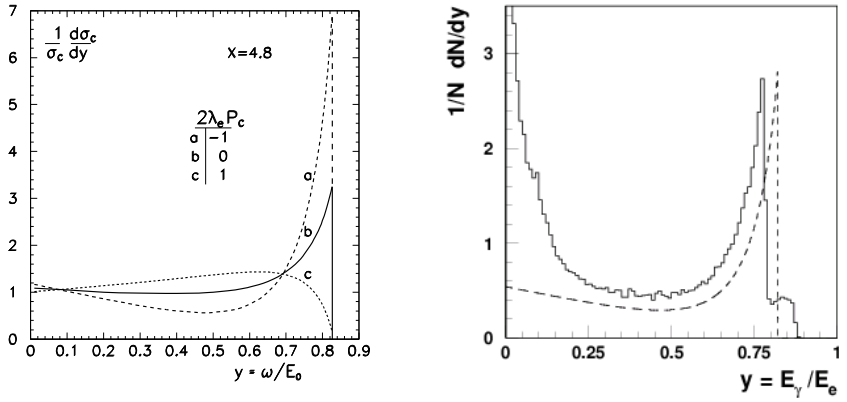

Fig. 1. Photon spectra. Left: The effect of electron/positron and laser photon polarization on the high-energy photon spectrum. Right: Experimental simulation of the photon spectrum including non-linear effects; Ref. [19].

2.2. Polarization

Circular polarization is transferred from the initial laser photons completely to the high energy photons for maximum energy at the peak of the spectrum, *cf.* Fig. 2 (left):

$$\lambda_\gamma \to -P_c \;\; [\text{near maximum}]. \tag{7}$$

Linear polarization responds less favorably, *cf.* Fig. 2 (right). The degree of polarization transferred from the laser to the high energy photons is reduced with rising photon energy, *i.e.* rising x:

$$l_\gamma \to +\frac{P_l}{[x^2/2(x+1)+1]} \ \text{[near maximum]}. \tag{8}$$

The variety of polarization states of the high energy photons makes the photon collider an ideal instrument for investigating the external spin-parity quantum numbers of particles [20] such as Higgs bosons, and for the study of CP violation effects [9].

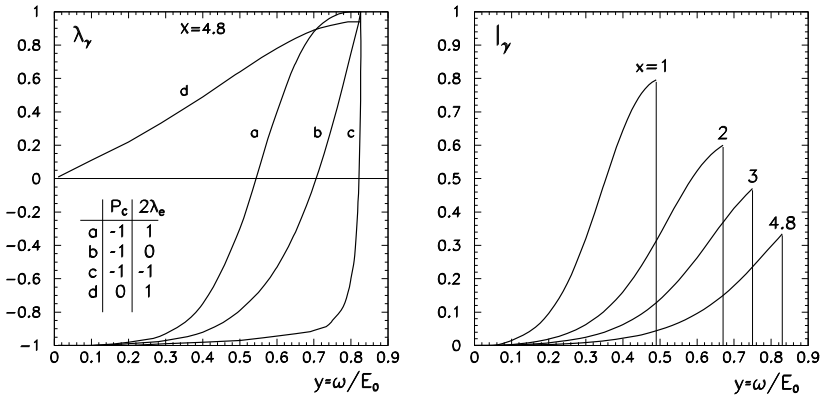

Fig. 2. The transfer of circular (left) and linear (right) laser γ polarization to the high-energy photons.

2.3. Luminosities and cross sections

The essential characteristics of the $e\gamma$ and $\gamma\gamma$ luminosity distributions can be determined by convoluting the photon spectrum with the electron spectrum and with itself, respectively.

The $e\gamma$ luminosity distribution coincides with the high-energy photon energy spectrum. Denoting the scaled $e\gamma$ invariant mass by $m_{e\gamma} = M_{e\gamma}/\sqrt{s}$, it is given by

$$\frac{d\mathcal{L}}{dm^2_{e\gamma}} = F(y = m^2_{e\gamma})\,. \tag{9}$$

The $\gamma\gamma$ luminosity distribution, on the other hand, is determined by the standard self-convolution of the photon spectrum. Denoting the $\gamma\gamma$ invariant mass by $m_{\gamma\gamma} = M_{\gamma\gamma}/\sqrt{s}$, the luminosity can be written as

$$\frac{d\mathcal{L}}{dm^2_{\gamma\gamma}} = \int\limits_{m^2_{\gamma\gamma}}^{1} \frac{dy}{y}\, F(y)\, F\left(m^2_{\gamma\gamma}/y\right)\,. \tag{10}$$

If the helicities of the laser photons and the electrons are chosen opposite to each other, a large fraction of the luminosity is accumulated in the high-energy region, *cf.* Fig. 3. For a polarization degree of 85% of the initial electrons and maximal polarization of the laser photons, the values of the $e\gamma$ and $\gamma\gamma$ luminosities are displayed in Table I in units of $10^{34}\text{cm}^{-2}\text{s}^{-1}$. About one third of the corresponding e^+e^- luminosity is accumulated within a margin of 20% below the maximum invariant energy:

$$\mathcal{L}_{\gamma\gamma}(\geq 0.8) \sim \frac{1}{3}\mathcal{L}_{ee}\,. \tag{11}$$

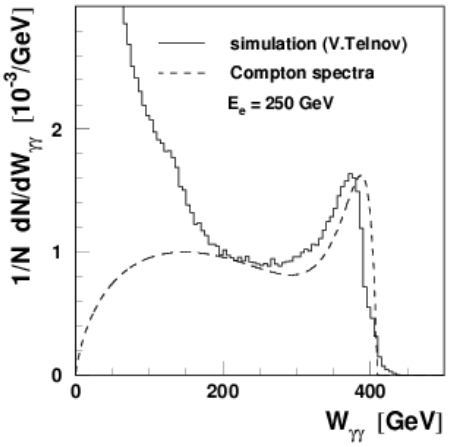

Fig. 3. Luminosity distribution of the $\gamma\gamma$ collider; Ref. [1].

TABLE I

Luminosities for $e\gamma$ and $\gamma\gamma$ within a margin of size 0.2 below the maximum invariant energies, compared with the LC e^+e^- luminosity; Ref. [1].

$\sqrt{s}_{ee}$ [GeV]	500	800
$m_{e\gamma} \geq 0.8 m_{e\gamma}^{\max}$	0.9	1.3
$m_{\gamma\gamma} \geq 0.8 m_{\gamma\gamma}^{\max}$	1.1	1.7
e^+e^-	3.4	5.8

Since the cross sections for the $e\gamma$ and $\gamma\gamma$ processes are significantly larger than the e^+e^- annihilation cross sections, the event rates are predicted of similar size for all three types of collisions.

A sample of cross sections for $\gamma\gamma$ processes is collected in Fig. 4. Since the size of the cross sections is large, extending from 10 to 10^5 fb, a large number of 10^3 to 10^7 events can be observed for a total integrated luminosity of 100 fb^{-1} in the high-energy margin of the luminosity distribution.

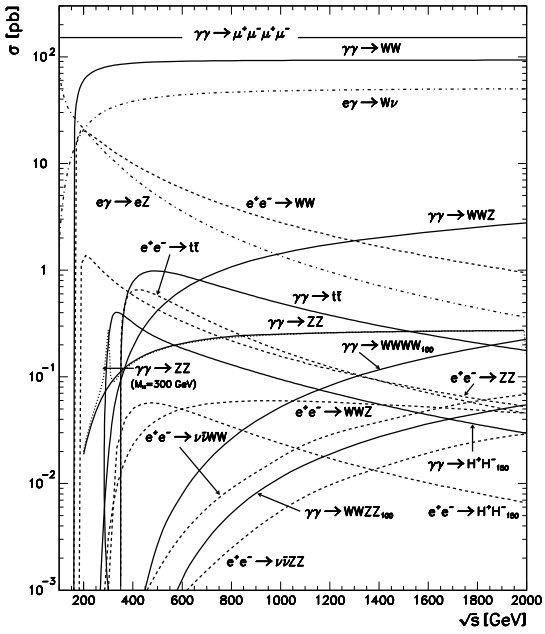

Fig. 4. Cross sections for $e\gamma$ and $\gamma\gamma$ processes as functions of the energy; compared with e^+e^- annihilation channels.

3. Electroweak symmetry breaking

The discovery of the mechanism which breaks the electroweak symmetries and the exploration of its nature are among the central experimental tasks at the next-generation high-energy colliders. The Higgs mechanism is strongly supported by high-precision analyses in the electroweak sector. However, these measurements can still be interpreted within a large variety of models incorporating different realizations of the Higgs mechanism. They extend from the Standard Model to embeddings in supersymmetric theories up to theories of extra space dimensions. A photon collider can contribute to the task of uncovering the underlying structure. The Higgs coupling to two photons, measured by the size of the Higgs formation cross section in photon collisions, is sensitive to high scales in the theory. Moreover, photon collisions provide unique opportunities for the discovery of the heavy

Higgs bosons in supersymmetric theories. Alternatively, strong electroweak symmetry breaking may be studied by measuring the static electromagnetic properties of the $W^{\pm}$ bosons in $\gamma\gamma$ fusion. These opportunities will be illustrated by a few typical examples.

3.1. Light Higgs in $\gamma\gamma$ collisions

The coupling of Higgs bosons to photons [21] is mediated by loops of charged particles. In the Standard Model the main contributions are generated by top quark and W boson loops. In scenarios beyond the Standard Model also heavier particles can contribute but the loops are suppressed with increasing masses according to the rules of quantum mechanics. (The suppression can be counter-balanced by rising Higgs couplings to the new particles if their masses are generated by the Higgs mechanism; however, for masses beyond $\sim 1/2$ TeV the theory would become strongly interacting and the perturbative loop argument would cease to be valid.)

The Higgs–$\gamma\gamma$ coupling determines the formation cross section of Higgs bosons in $\gamma\gamma$ fusion. Apart from normalization, the cross section can conveniently be expressed by the partial $\gamma\gamma$ decay width of the Higgs boson and the luminosity function; for narrow Higgs bosons:

$$\sigma_{\gamma\gamma} \sim \Gamma_{\gamma\gamma}\, d\mathcal{L}/dm^2_{\gamma\gamma}\,(M_H^2)\,. \tag{12}$$

Choosing the helicities of the photons opposite to each other enhances the signal and helps suppress the background. The Higgs boson can be detected either as a peak in the invariant mass distribution, *e.g.* in $b\bar{b}$ or ZZ decays, or by scanning, taking advantage of the sharp upper edge of the $\gamma\gamma$ spectrum. b decays are leading below a Higgs mass of 140 GeV; Z decays, for which the

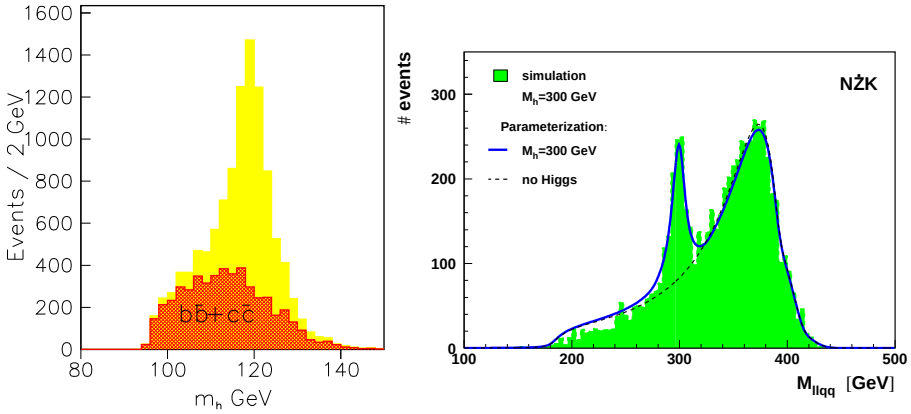

Fig. 5. Final state invariant bb, ZZ masses for light and heavy Higgs boson production in $\gamma\gamma$ collisions; Refs. [4, 5], respectively.

background is strongly suppressed compared to W decays, can be used for heavy Higgs masses, *cf.* Fig. 5. In the lower mass region the partial width can be measured with an accuracy of 2.1% [4].

If the $H \to \gamma\gamma$ decay branching ratio is measured in Higgs-strahlung, the ratio $\tau_H = \mathrm{BR}_{\gamma\gamma}/\Gamma_{\gamma\gamma}$ determines the lifetime τ_H of the Higgs boson. Depending on the error of the branching ratio [22], an accuracy between 15 and 5% may be reached, matching eventually the WW channel.

3.2. Beyond the Standard Model (I)

The high precision in the measurement of the Higgs-$\gamma\gamma$ coupling may be exploited to determine or, at least, constrain high scales in theories beyond the Standard Model in which the Higgs mechanism may be embedded.

In 2-Higgs doublet models a situation could arise in which all the properties of the lightest Higgs boson observed at LHC and ILC may be in concordance with SM expectations but the heavy Higgs bosons may not have been observed yet. In this situation the measurement of the $\gamma\gamma$ width can discriminate the extended Higgs model from the Standard Model [23]. Deviations of the $\gamma\gamma$ width from the Standard Model by more than a factor two could still be possible and they could easily be detected at a photon collider.

In models including triplet Higgs fields, doubly charged Higgs bosons will be generated in addition to the singly charged Higgs bosons of 2-doublet Higgs models. The double electric charge increases the production cross section by a factor 16 over the cross section for singly charged Higgs bosons.

In Little Higgs models deviations from the Standard Model are predicted across the interesting range of the scale parameter f [24]. Moreover, the breaking of anomalous U(1) gauge symmetries may generate new axion-type scalar particles [25] which can be searched for, as narrow states, in channels parallel to the Higgs bosons, *cf.* Fig. 6.

Potentially large modifications of the Higgs–$\gamma\gamma$ coupling are expected quite generally in models with strong electroweak symmetry breaking [26]. If the photons couple directly to constituents of the Higgs boson, the $\gamma\gamma$ branching ratio can rise to values significantly above the Standard Model value and may even become dominant, depending on the size of the confinement parameters of the Higgs constituents.

In theories of extra space dimensions, the Kaluza–Klein states may alter the Higgs–$\gamma\gamma$ coupling [27]. In addition, in specific models, like Randall–Sundrum type (RS) models, the radion field may mix with the Higgs field and the properties of the Higgs particle may be modified significantly; for details see *e.g.* Ref. [28].

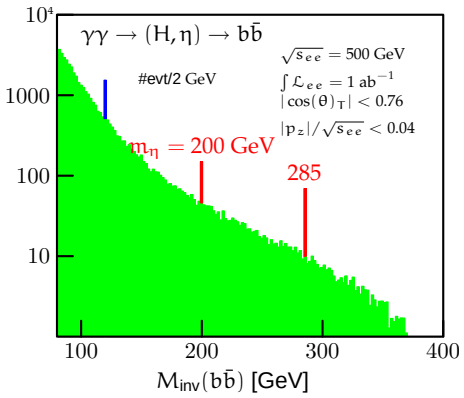

Fig. 6. The formation of an axion-type particle η of Little Higgs models in addition to the Higgs particle in $\gamma\gamma$ collisions; Ref. [25].

3.3. Beyond the Standard Model (II): supersymmetry Higgs sector

The contribution of charged supersymmetric particles to the loops in the Higgs–$\gamma\gamma$ coupling can give rise to noticeable effects, *cf.* Ref. [29], if the particles are not too heavy.

Heavy Higgs Bosons: If supersymmetry is realized in nature, a photon collider could be a unique instrument for exploring the Higgs sector of the theory. In the wedge centered around medium values of $\tan\beta$ beyond masses of about 200 GeV heavy Higgs bosons cannot be discovered at LHC and beyond 300 GeV even not at SLHC. Nor can the Higgs particles be discovered at the e^+e^- linear collider beyond 250 GeV and 500 GeV in the first phase and the second phase, respectively, as heavy scalar+pseudoscalar particles are produced in pairs. Thus only the lightest Higgs particle would be detected in standard channels while the other members of the Higgs spectrum would remain undiscovered. This wedge however can be covered in the $\gamma\gamma$ mode of the linear collider,

$$\gamma\gamma \to H, A \tag{13}$$

which extends the mass reach in formation experiments to about 80% of the total e^+e^- energy [6], *i.e.* up to 400 GeV and 800 GeV in the first and second phase of the operation. A clear Higgs signal can be isolated above the background [7] as demonstrated in Fig. 7.

Besides the discovery of heavy Higgs bosons, a photon collider could be very valuable if not even unique in determining some of the parameters in the Higgs sector of supersymmetric theories.

Higgs Mixing $\tan\beta$: The measurement of the mixing parameter $\tan\beta$ is a difficult task for large values. Noticing that the Higgs Yukawa couplings to τ pairs are of the order of $\tan\beta$, the splitting of high-energy photons to τ's can be exploited to measure this parameter in $\tau\tau$ fusion, *cf.* Ref. [30]:

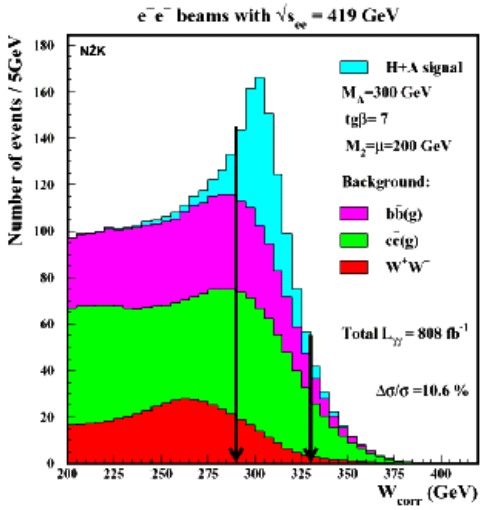

Fig. 7. Experimental simulation of the production of heavy Higgs bosons at a photon collider in supersymmetric theories [7].

$$\sigma[\gamma\gamma \to \tau\tau + h/H/A] \;\sim\; \tan^2\beta\,. \tag{14}$$

For moderate A, H masses, the $h\tau\tau$ coupling is of the order of $\tan\beta$, while for large A, H masses the size of the $A\tau\tau$ and $H\tau\tau$ couplings is determined by this parameter; thus the entire mass parameter range can be covered. Since the splitting function of photons to leptons is hard, the energy of the τ beams is high so that Higgs particles with large masses can be produced. Introducing proper cuts to suppress the backgrounds, an accuracy of

$$\Delta\tan\beta = 0.9 \text{ to } 1.3\,, \tag{15}$$

can be expected across the entire medium to large $\tan\beta$ range [30].

CP Violation: The 2-doublet Higgs sector of the minimal supersymmetric extension of the Standard Model is automatically CP conserving at the tree level. However, CP violation [9, 31] can be induced by radiative corrections transmitting CP-violating phases from the soft SUSY breaking Lagrangian to the Higgs system, in particular the relative phases between the Higgsino mass parameter μ and the trilinear sfermion-Higgs parameter $A_{\rm f}$.

CP asymmetries are naturally enhanced [9] in the decoupling regime where $M_A \simeq M_H$. The near mass degeneracy of the scalar and pseudoscalar states allows for frequent mutual transitions which induce large CP-odd mixing effects in CP-violating theories. This is quantitatively described by the complex mixing parameter

$$\frac{1}{2}\tan 2\theta = \frac{\Delta^2_{HA}}{M^2_H - M^2_A - i[M_H\Gamma_H - M_A\Gamma_A]}\,, \tag{16}$$

where the off-diagonal CP-violating parameter Δ_{HA} in the Higgs mass matrix couples the two states.

The asymmetry between left- and right-handedly polarized top quark pairs, produced in $\gamma\gamma$ fusion on the top and in the Breit–Wigner wings of the Higgs bosons, signals these CP-violating effects [8].

However, CP violation can be studied in a classical way by measuring asymmetries of inclusive cross sections between left- and right-polarized photons [9]:

$$A_{\rm LR} = \frac{\sigma_{++} - \sigma_{--}}{\sigma_{++} + \sigma_{--}} \,. \tag{17}$$

Remarkably large asymmetries are predicted on top of the Higgs bosons in $\gamma\gamma$ fusion, shown in Fig. 8 as a function of the CP-violating phase of the trilinear stop-Higgs coupling $A_{\rm t}$.

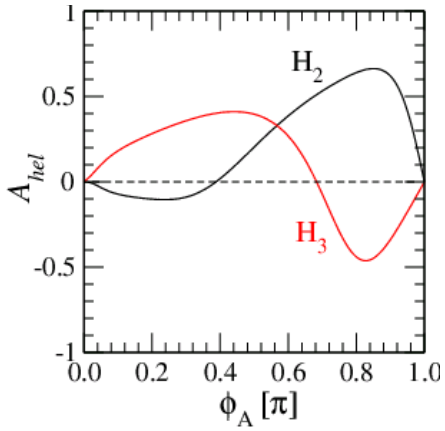

Fig. 8. LR asymmetries predicted in CP non-invariant supersymmetric theories on top of the two heavy Higgs bosons in $\gamma\gamma$ collisions; Ref. [9].

3.4. Strongly interacting W bosons

If electroweak symmetry breaking is generated dynamically by new strong interactions at a scale not far above 1 TeV, the longitudinal degrees of the W bosons, which are equivalent to the Goldstone bosons associated with spontaneous symmetry breaking, become strongly interacting particles. As a result, the properties of the W bosons will be affected by the nearby new strong interactions. In particular deviations are expected in such a scenario for the static electroweak parameters from the values which are generated by the electroweak gauge interactions of the Standard Model:

$$\begin{aligned} \text{magnetic } W^{\pm} \text{ dipole moment} &: \mu_W = 2 \times e/2M_W \,, \\ \text{electric } W^{\pm} \text{ quadrupole moment} &: Q_W = -e/M_W^2 \,. \end{aligned}$$

The deviations are described by linear combinations of parameters $\Delta\kappa_\gamma$ and λ_γ which modify the $WW\gamma$ vertex.

This modification can be studied [14] in the process

$$\gamma\gamma \to W^+W^- \,, \tag{18}$$

which receives large contributions from the t- and u-channel W exchanges. For a total energy of 800 GeV and an integrated luminosity of 1 ab^{-1}, the expected sensitivity for the parameters $\Delta\kappa_\gamma$ and λ_γ is shown in Table II, compared with the corresponding sensitivities in the e^+e^- mode. Apparently, the sensitivity on λ_γ at the $\gamma\gamma$ collider is superior to the e^+e^- collider, though not dramatically.

TABLE II

Sensitivity of WW pair production at $\gamma\gamma$ and e^+e^- colliders to the $WW\gamma$ vertex parameters in theories of strong electroweak symmetry breaking; Ref. [14].

	$\gamma\gamma : J_z = 2$	$\gamma\gamma : J_z = 0$	$e^+e^- : J_z = 1$
$\Delta\kappa_\gamma/10^{-4}$	5.2	13.9	2.1
$\lambda_\gamma/10^{-4}$	1.7	2.5	3.3

4. Supersymmetric particles

The genuine supersymmetric particle sector is the second domain of a photon collider for potentially unique discoveries of particles which cannot be observed at other colliders. In supersymmetric scenarios in which sfermions are heavy but charginos/neutralinos light, cascade decays, the prime source of non-colored particles at LHC, do not include sleptons at a significant rate. On the other hand, the sleptons may be too heavy to be produced in pairs in the e^+e^- mode of the linear collider. In this situation an $e\gamma$ collider could open the window to selectrons and e-sneutrinos [10,11].

While the energy in the e^+e^- mode must at least be larger than twice the mass of the lightest selectron,

$$e^+e^- \to \tilde{e}_i^+\tilde{e}_j^- \quad : \quad \min\left[m_{\tilde{e}}\right] \leq \frac{1}{2}\sqrt{s}\,, \tag{19}$$

the associated production of selectron and neutralino, or sneutrino and chargino, in the $e\gamma$ mode,

$$e\gamma \to \tilde{e}_i\tilde{\chi}_j^0 \quad \text{or} \quad \tilde{\nu}_{e_i}\tilde{\chi}_j^\pm \quad : \quad m_{\tilde{\ell}} \leq \sqrt{s} - m_{\tilde{\chi}}\,, \tag{20}$$

can give access to heavier selectrons and sneutrinos if the neutralinos and charginos are light, Fig. 9.

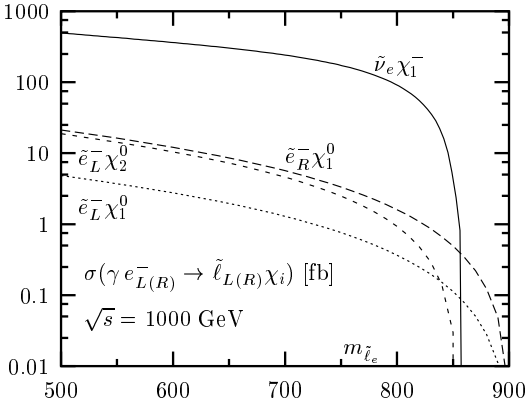

Fig. 9. Total cross sections for the associated production of first generation sleptons with charginos and neutralinos in $e^-\gamma$ collisions as functions of the slepton masses; *cf.* Ref. [10].

Due to t-channel slepton exchanges the processes set in sharply at the thresholds proportional to the velocities β. The fast rise of the cross section can be exploited in threshold scans to determine the masses quite accurately. In the SPS1a′ example shown in Fig. 10, the sneutrino mass can be measured with an accuracy of 3 GeV, *cf.* Ref. [11]. The accuracy is less than expected from chargino decays; however, all these experiments are quite involved due to numerous supersymmetry backgrounds to the supersymmetry signal so that cross checks are indispensable.

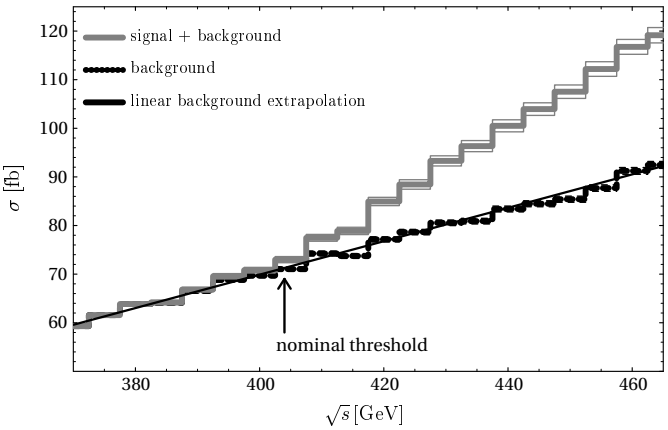

Fig. 10. Sneutrino mass measurement by scanning the threshold in the process $e\gamma \to \tilde{\nu}\tilde{\chi}$; Ref. [11].

5. Strong interactions and QCD

5.1. $\gamma\gamma$ fusion to hadrons

One of the most demanding areas for the understanding of QCD as the fundamental theory of the strong interactions is hadron production in $\gamma\gamma$ collisions. Perturbative mechanisms are superimposed on non-perturbative mechanisms with a difficult transition zone in between. Since photons can fluctuate to vector mesons, the standard Pomeron exchange will contribute to the process. On the other hand, fluctuations to quark–antiquark pairs at short distances will give rise to perturbative QCD components, *e.g.* perturbative hard Pomeron exchange and production of mini-jets in $\gamma\gamma$ collisions. While for energies in the former LEP range, the relative weight of the mechanisms could not be determined properly, the increase of the collision energy up to about 1 TeV at a photon collider is expected to discriminate between the various contributions. The theoretical picture is still evolving so that definite conclusions cannot be drawn yet at the present time [32].

5.2. Quark–gluon structure of the photon

The measurement of the photon structure functions [33] at an $e\gamma$ collider is of great theoretical interest. In contrast to the proton structure function, the main characteristics of the photon structure functions can be predicted theoretically. They are derived from the point-like splitting of photons to quark–antiquark pairs [15] which gives rise to the increase of the photon structure function F_2 for rising Bjorken-x and to its uniform increase in the logarithm of the momentum transfer $\log Q^2$, both features in sharp contrast to the proton. The QCD leading order corrections [16] modify the structure function in a characteristic way. The perturbative radiation of gluons alters the x dependence at $\mathcal{O}(1)$, though not overturning the characteristic rise in x, but it leaves the uniform $\log Q^2$ rise unchanged. This is a direct consequence of asymptotic freedom [34]; any other than the logarithmic Q^2 fall-off of the QCD coupling would have led to a power dependence of the structure function. The non-logarithmic terms of the structure function receive contributions from next-to-leading order of QCD [17] but remnants from the vector-meson like component of the photon preclude the perturbative prediction of the absolute normalization for non-asymptotic Q^2 values. Nevertheless, the theoretical prediction of the exceptional x dependence and the uniform $\log Q^2$ rise render deep-inelastic electron–photon scattering an exciting experimental task at an $e\gamma$ collider.

Neutral and charged-current mechanisms can be used to determine the quark–parton content of the photon over a wide range of Q^2:

$$\begin{aligned} e\gamma \to eX \quad &: \quad F_2^{\mathrm{n}} \sim [4(u+c)+(d+s)]\,, \\ e\gamma \to \nu X \quad &: \quad F_{2,3}^{\mathrm{c}} \sim [(u+c)\pm(d+s)]\,. \end{aligned} \tag{21}$$

Range and accuracy with which F_2 can be measured are shown in Fig. 11, Ref. [35]. The analysis of charged-current deep-inelastic scattering allows the separation of up- and down-quark components of the photon [36].

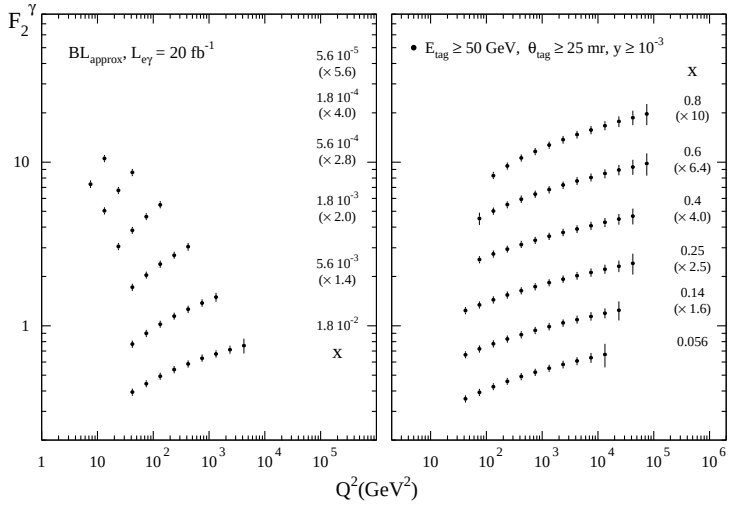

Fig. 11. Accuracy with which the photon structure function F_2 can be measured over a wide area in the (x, Q^2) plane; Ref. [35].

The vector–meson component of the photon as well as perturbative gluon radiation suggest a gluon component within the photon. The (x, Q^2) dependence of the gluon component can be determined in two ways. First, the $\log Q^2$ evolution of the photon structure function is affected by the splitting of gluons to quark–antiquark pairs [37]. Second, part of the high-transverse momentum jets in $e\gamma$ scattering

$$e\gamma \to e + j + X\,, \tag{22}$$

are generated at the microscopic level by the subprocess

$$\gamma^* + g \to q + \bar{q}\,. \tag{23}$$

Studying the rapidity and transverse-momentum distributions of the jets j can thus be used to measure the gluon distribution of the photon after the quark and anti-quark initiated Compton jets are subtracted [38].

Finally, the spin structure function of the photon, $g_1(x, Q^2)$, can be measured in deep-inelastic scattering of longitudinally polarized electrons on circularly polarized photons. As shown earlier, circular polarization can be realized to a high degree for the photon beams. In next-to-leading order the structure function g_1 can be predicted in the asymptotic regime, the result matched closely by predictions based on standard evolution procedures [39].

6. Summary

A photon collider provides us with an experimental instrument with which a large variety of problems across the entire range of physics beyond the Standard Model can be addressed. Moreover, within the Higgs sector and the slepton sector of supersymmetric theories such a collider may give unique access to heavy Higgs particles and heavy selectrons and e-sneutrinos. Thus, by not only offering a platform for studying a rich experimental bouquet of interesting problems but also providing unique physics opportunities, a photon collider can be considered a valuable component of a future linear collider program.

REFERENCES

[1] B. Badelek *et al.* (ECFA/DESY Photon Collider Working Group), "TESLA Technical Design Report, Part VI: Photon Collider", *Int. J. Mod. Phys.* **A19**, 5097 (2004) [hep-ex/0108012].

[2] E. Boos *et al., Nucl. Instrum. Methods* **A472**, 100 (2001) [hep-ph/0103090].

[3] I. Ginzburg *et al., Pisma Zh. Eksp. Teor. Fiz.*, **34**, 514 (1981); *JETP Lett.* **34**, 491 (1981); I. Ginzburg *et al., Nucl. Instrum. Methods* **205**, 47 (1983); I. Ginzburg *et al., Nucl. Instrum. Methods* **219**, 5 (1984).

[4] K. Monig, A. Rosca, hep-ph/0506271.

[5] P. Niezurawski, A.F. Zarnecki, M. Krawczyk, *J. High Energy Phys.* **0211**, 034 (2002) [hep-ph/0207294].

[6] M.M. Muhlleitner, M. Kramer, M. Spira, P.M. Zerwas, *Phys. Lett.* **B508**, 311 (2001) [hep-ph/0101083].

[7] P. Niezurawski, A.F. Zarnecki, M. Krawczyk, hep-ph/0507006.

[8] E. Asakawa, S.Y. Choi, K. Hagiwara, J.S. Lee, *Phys. Rev.* **D62**, 115005 (2000) [hep-ph/0005313]; E. Asakawa, K. Hagiwara, *Eur. Phys. J.* **C31**, 351 (2003) [hep-ph/0305323].

[9] S.Y. Choi, J. Kalinowski, Y. Liao, P.M. Zerwas, *Eur. Phys. J.* **C40**, 555 (2005) [hep-ph/0407347].

[10] F.M. Renard, *Z. Phys.* **C14**, 209 (1982); A. Datta, A. Djouadi, M. Muhlleitner, *Eur. Phys. J.* **C25**, 539 (2002) [hep-ph/0204354].

[11] A. Freitas, W. Porod, P.M. Zerwas, *Phys. Rev.* **D** in press, hep-ph/0509056.

[12] B. Grzadkowski, Z. Hioki, K. Ohkuma, J. Wudka, hep-ph/0511038.

[13] S.Y. Choi, F. Schrempp, *Phys. Lett.* **B272**, 149 (1991); O. Nachtmann, F. Nagel, M. Pospischil, A. Utermann, hep-ph/0508132 and hep-ph/0508133; G.J. Gounaris, hep-ph/0510061.

[14] K. Monig, J. Sekaric, hep-ex/0507050.

[15] T.F. Walsh, P.M. Zerwas, *Phys. Lett.* **B44**, 195 (1973).

[16] E. Witten, *Nucl. Phys.* **B120**, 189 (1977).

[17] W.A. Bardeen, A.J. Buras, *Phys. Rev.* **D20**, 166 (1979); Erratum **D21**, 2041 (1980).

[18] S. Bray, J.S. Lee, A. Pilaftsis, *Phys. Lett.* **B628**, 250 (2005) [hep-ph/0508077].

[19] V.A. Telnov, ECFA/DESY LC Workshop, Saint Malo 2002; A.F. Zarnecki, *Acta Phys. Pol. B* **34**, 2741 (2003).

[20] M. Kramer, J.H. Kuhn, M.L. Stong, P.M. Zerwas, *Z. Phys.* **C64**, 21 (1994) [hep-ph/9404280].

[21] J.F. Gunion, H.E. Haber, G.L. Kane, S. Dawson, hep-ph/9302272.

[22] A. Battaglia, T. Barklow, M.E. Peskin, Y. Okada, S. Yamashita, P.M. Zerwas, "Physics Benchmarks for the ILC Detectors", LCWS2005, Stanford 2005 [in press].

[23] I.F. Ginzburg, M. Krawczyk, P. Osland, *Nucl. Instrum. Methods* **A472**, 149 (2001) [hep-ph/0101229].

[24] H.E. Logan, *Phys. Rev.* **D70**, 115003 (2004) [hep-ph/0405072].

[25] W. Kilian, D. Rainwater, J. Reuter, *Phys. Rev.* **D71**, 015008 (2005) [hep-ph/0411213].

[26] T. Han, in "Higgs Report — Proceedings, 2005 Snowmass Workshop".

[27] B. Lillie, hep-ph/0505074.

[28] J.F. Gunion, hep-ph/0410379.

[29] A. Djouadi, hep-ph/0503173.

[30] S.Y. Choi, J. Kalinowski, J.S. Lee, M.M. Muhlleitner, M. Spira, P.M. Zerwas, *Phys. Lett.* **B606**, 164 (2005) [hep-ph/0404119].

[31] R.M. Godbole, S.D. Rindani, R.K. Singh, *Phys. Rev.* **D67**, 095009 (2003); Erratum **D71**, 039902 (2005) [hep-ph/0211136].

[32] G. Pancheri, *Acta Phys. Pol. B* **37**, 1093 (2006), these proceedings.

[33] S.J. Brodsky, T. Kinoshita, H. Terazawa, *Phys. Rev. Lett.* **27**, 280 (1971); T.F. Walsh, *Phys. Lett.* **B36**, 121 (1971).

[34] P.M. Zerwas, in Proceedings of "XV International Symposium on Multiparticle Dynamics", Lund 1984; C. Peterson, P.M. Zerwas, T.F. Walsh, *Nucl. Phys.* **B229**, 301 (1983).

[35] A. Vogt, A. De Roeck, in Ref. [1].

[36] A. Gehrmann-De Ridder, H. Spiesberger, P.M. Zerwas, *Phys. Lett.* **B469**, 259 (1999) [hep-ph/9909230].

[37] S.J. Brodsky, M. Kramer, P.M. Zerwas, *Nucl. Phys. Proc. Suppl.* **B37**, 293 (1994).

[38] T. Wengler, A. De Roeck, *Nucl. Instrum. Methods* **A472**, 217 (2001) [hep-ph/0010293].

[39] M. Stratmann, W. Vogelsang, *Phys. Lett.* **B386**, 370 (1996) [hep-ph/9606346].